










RESEARCH ARTICLE | AUGUST 20 2025

## A compact tabletop extreme-ultraviolet source for polarization-sensitive ptychographic imaging

Taylor J. Buckway ; Aaron Redd ; Hyrum Taylor ; Jacob Feltman ; Kaylee Nyborg ;  
J. Nicholas Porter ; Joshua A. Miller ; David Allred ; Richard L. Sandberg 



*Rev. Sci. Instrum.* 96, 083706 (2025)

<https://doi.org/10.1063/5.0274295>



View  
Online



Export  
Citation



**MCL**  
MAD CITY LABS INC.

Closed Loop Nanopositioning Systems with Picometer precision, Low noise and High stability

Force Microscopy and Single Molecule Microscopy Instruments for Quantum, Materials, and Bioscience

Custom Design and Innovative Solutions for the Nanoscale World

Think Nano® | Positioning | Microscopy | Solutions



# A compact tabletop extreme-ultraviolet source for polarization-sensitive ptychographic imaging

Cite as: Rev. Sci. Instrum. 96, 083706 (2025); doi: 10.1063/5.0274295

Submitted: 4 April 2025 • Accepted: 27 July 2025 •

Published Online: 20 August 2025



Taylor J. Buckway,<sup>a)</sup> Aaron Redd, Hyrum Taylor, Jacob Feltman, Kaylee Nyborg, J. Nicholas Porter, Joshua A. Miller, David Allred, and Richard L. Sandberg

## AFFILIATIONS

Department of Physics and Astronomy, Brigham Young University, Provo, Utah 84604, USA

<sup>a)</sup> Author to whom correspondence should be addressed: [taylorbuckway@gmail.com](mailto:taylorbuckway@gmail.com)

## ABSTRACT

Extreme-ultraviolet light has become more important for advancements in modern computer chip manufacturing, and as such, there needs to be more access to extreme-ultraviolet sources for observing properties of novel technology materials. Some of these extreme-ultraviolet sources need to have the ability to tune the polarization for observing dichroic properties of materials such as magnetism. We present a compact extreme-ultraviolet tabletop source, based on high harmonic generation, designed for use in polarization-sensitive imaging. The source is able to generate circularly polarized harmonics using the MACH-ZEHNDER-LESS for Threefold Optical Virginia spiderwort apparatus. The linearly polarized 42 and 52 eV beams have been optimized, achieving an average power of 19.4 and 8.0 nW, respectively. Using the 42 eV linearly polarized beam for ptychography, we have imaged a Siemens star test resolution target and obtained a resolution of 160 nm.

Published under an exclusive license by AIP Publishing. <https://doi.org/10.1063/5.0274295>

## I. INTRODUCTION

Extreme-ultraviolet (EUV) light has become increasingly important due to modern computer chip manufacturing using EUV lithography to produce ever smaller critical dimensions for faster, lower-power electronics.<sup>1,2</sup> In addition, EUV light has pushed science to the shortest time scales by exploring attosecond physics, an accomplishment that was recognized by the 2023 Nobel Prize in Physics.<sup>3</sup> EUV and soft x-ray (SXR) light have photon energies that are resonant with several shallow core electrons, which provides elemental sensitivity.<sup>1</sup> This resonant capability enables many powerful techniques, such as enabling element specific imaging of buried interfaces<sup>4,5</sup> and enhanced resonant magnetic spectroscopy, scattering, and imaging.<sup>6,7</sup> Probing the magnetic order with EUV/SXR radiation requires dichroic absorption or reflection that is dependent on the polarization and wavelength of the light and is sensitive to the local magnetic order in the material of interest.<sup>6</sup> This property is used in studying magnetism using magnetic circular dichroism (MCD) or magnetic linear dichroism (MLD),<sup>8–10</sup> EUV/SXR reflectometry,<sup>11</sup> and ferroelectric polarization using linear EUV/SXR dichroism.<sup>12</sup>

Traditionally, large accelerator-based photon facilities, such as synchrotrons, were the primary sources for EUV/SXR light.<sup>1</sup> More

recently, tabletop sources have expanded access to the EUV/SXR spectral range.<sup>13–20</sup> One such tabletop EUV source is based on high harmonic generation (HHG). HHG is an extremely nonlinear optical process that converts ultrafast, high-intensity, near-infrared, or optical laser pulses into EUV (10–100 eV) and soft x-ray (100–1000 eV) radiation.<sup>21–23</sup> The infrared (IR) or optical laser pulses are focused into a noble gas medium and converted to EUV/SXR radiation through an extreme nonlinear upconversion process. The efficiency of this up-converted short wavelength light depends on phase-matching parameters such as gas pressure, intensity of the driving laser beam, and the geometry of the HHG system.<sup>24–26</sup>

Several developments in HHG, including brighter and more coherent EUV beams,<sup>22,27–34</sup> beam stabilization,<sup>35,36</sup> and the generation of circularly polarized EUV light,<sup>16,37–40</sup> provide increased avenues for probing the properties of materials. Circularly polarized EUV light from HHG is generated using a bi-circularly (one left and one right) polarized, bi-chromatic (two-color) beam. The bi-chromatic beam consists of IR wavelengths and their second harmonic (~400 nm). The combined electric field forms a three-fold flower pattern that allows the ionized electrons to return to their parent atoms and, thus, generate circularly polarized harmonics.<sup>37–39</sup>

The harmonic generation process must follow the conservation of energy, momentum, and photon angular momentum.<sup>37,41</sup> The energy of the generated harmonic must be equal to the sum of the energies of the driving fundamental (IR) and second harmonic photons (blue) ( $\hbar\omega_n = \hbar\omega_{IR} + n\hbar\omega_{blue}$ ). Conservation of intrinsic angular momentum requires the total angular momentum to be the same before and after harmonic generation. A photon can have an angular momentum of either +1 or -1, or in other words, the photon can be left or right circularly polarized. Thus, right circularly polarized beams are made up of photons with +1 angular momentum, and left circularly polarized beams are made up of photons with -1 angular momentum.

In order to obtain circularly polarized high harmonics from a bi-chromatic beam, the number of fundamental photons must be one more than or one less than the number of second harmonic photons ( $l = n \pm 1$ ). These requirements together determine the allowed circularly polarized harmonics given as  $\hbar\omega_n = (3n \pm 1)\hbar\omega_{IR}$ . The high harmonic circularly polarized spectrum has harmonic pairs in which every third harmonic is forbidden.<sup>37,39,41</sup>

Several magnetic experiments have been performed using circularly polarized HHG sources, the majority of which were done with spectroscopy.<sup>14,15,42</sup> There are only a few examples of dichroic magnetic imaging with HHG sources. Dichroic magnetic imaging with HHG sources has been performed by combining the principles of Fourier transform holography and coherent diffraction imaging (CDI).<sup>16,40</sup> A scanning CDI technique known as ptychography can be used to image extended specimens.<sup>43–47</sup> Yet, ptychography has not been successfully demonstrated with dichroic magnetic imaging with HHG sources, although it has been accomplished at large x-ray facilities.<sup>48,49</sup> HHG sources have beam variations such as intensity fluctuations and pointing instabilities due to the highly nonlinear generation process. These beam fluctuations pose convergence challenges for ptychographic algorithms.<sup>50</sup> Several techniques have been presented to address these instabilities by stabilizing the beam or correcting the instabilities using relaxation models in the ptychographic image reconstruction algorithms.<sup>47,51,52</sup> In this work, we present our EUV tabletop source designed for high-resolution polarization-sensitive imaging. We present the design of the HHG

system, its capabilities (including polarization control and selection of harmonics), and our first ptychography imaging result. We also include in the [Appendix](#) a detailed approach to aligning the MAZEL-TOV (Mach-Zehnder-Less for Threefold Optical Virginia spiderwort) apparatus.<sup>39</sup>

## II. POLARIZATION SENSITIVE EUV IMAGING SETUP

The EUV HHG source is shown in [Fig. 1](#). A Solstice Ace Ti:sapphire laser is used to drive the HHG process. The laser has 800 nm central wavelength with a 30 nm bandwidth, a pulse duration of 35-fs, a maximum pulse energy of 7 mJ, and a repetition rate of 1 kHz. The laser has the capability to adjust the pulse duration by inducing spectral chirp by introducing a quadratic phase in the ultrafast pulse. Chirping the driving laser pulse causes an energy shift of the EUV spectrum.<sup>34,53</sup> This allows for fine-tuning of the EUV beam, which assists in energy-sensitive processes such as MCD and MLD. The laser is focused using a 1500 or 1000 mm lens into a gas cell shown in [Fig. 2](#). In order to control the polarization of the EUV pulses, we use a removable MAZEL-TOV apparatus. The MAZEL-TOV produces the bi-circular, bi-chromatic beam for generating the circularly polarized harmonics. More details about the MAZEL-TOV, including how it can be used to generate circularly polarized high harmonics, are in the original publication by Kfir *et al.*<sup>39</sup> It consists of four optics: a  $10 \times 10 \times 1$  mm<sup>3</sup> BBO (barium borate) crystal cut at  $\theta = 29.2^\circ$  and  $\phi = 90^\circ$  for type II phase-matching (Eksma Optics BBO-1004H), two delay-compensation plates (Eksma Optics 225-2114), and a multiple order dual-band quarter-wave plate (Eksma Optics 463-4441). Our MAZEL-TOV is a removable apparatus set on a magnetic kinematic base as shown in the photograph inset in [Fig. 1](#). The calcite plates are mounted on rotation stages (Thorlabs MSRP01), which are attached to the base such that the teeth of the stages interlock, making it convenient to tilt both calcite plates simultaneously. The dispersion through the four optics of the MAZEL-TOV can be precompensated by adjusting the compressor of the Ti:sapphire laser so that the blue frequencies are shifted ahead of the red frequencies in the 35 fs pulse. After the gas cell, the bi-chromatic laser driving beam is removed by thin

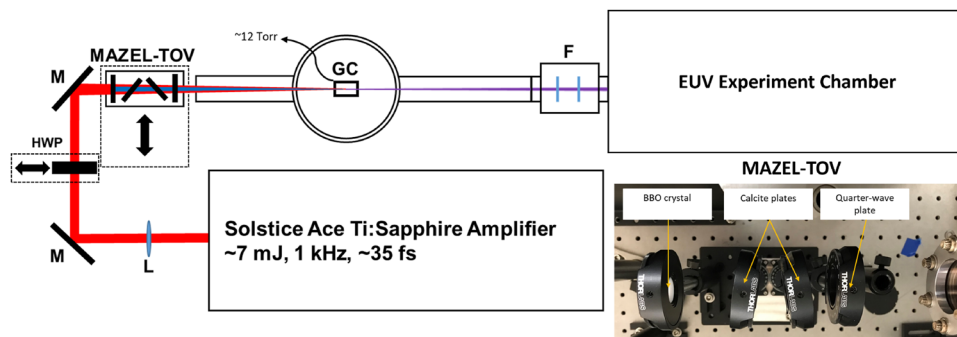


**FIG. 1.** Design of our EUV tabletop source with polarization control. The Ti:sapphire laser beam is directed using mirrors **M** and then focused using a lens **L** into a gas cell (**GC**) containing argon gas. The unspent driving fundamental beam is blocked using thin metal filters **F** mounted in two filter wheels. The generated EUV beam then propagates into the experiment chamber. The MAZEL-TOV apparatus can be inserted upstream of the vacuum chamber to produce the bi-chromatic beam needed to generate the circularly polarized EUV beam. An insertable half-wave plate (**HWP**) ensures proper IR polarization for the MAZEL-TOV apparatus.

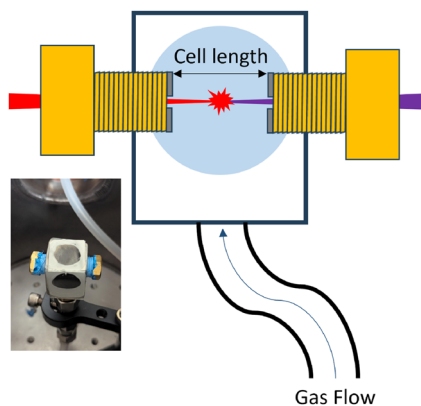


**FIG. 2.** Finite gas cell design for generating high harmonics. The gas cell is a machined aluminum box with threaded holes, which are for hollowed brass pipe fittings (yellow–orange). 0.1 mm molybdenum sheets (shown in gray) are attached to the ends of the brass fittings using Torr Seal. The brass fittings are then inserted into the threaded holes of the gas cell. The gas cell length (5–15 mm) is determined from the separation distance between the molybdenum sheets. The laser drills ~0.2–0.8 mm holes through the molybdenum sheets. Argon gas (99.997% purity) is pumped into the gas cell as shown with the line attached to the bottom of the gas cell. A window (light blue circle) is attached to another opening at the top and sides of the gas cell for observing the beam in the gas cell.

metal aluminum filters (Lebow Company, 200 nm foil thickness, 10 mm aperture diameter, part number 0.2Al-0-C10mm; 100 nm foil thickness, 10 mm aperture diameter, part number 0.1Al-0-C10mm). These filters remove unwanted light outside the energy range of 20–72 eV.

The experimental chamber has two configurations shown in Fig. 3: (a) a set of multilayer normal incidence mirrors and (b) a spectrometer. In configuration (a), the set of multilayer mirrors is designed to reflect either 42 or 52 eV light. The 42 eV mirror has a

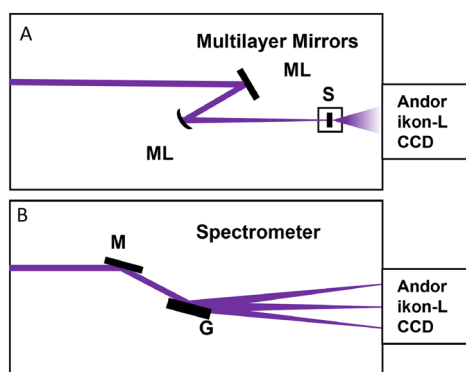


**FIG. 3.** (a) Normal incidence multilayer mirrors (ML) are primarily used for ptychographic imaging. The mirrors are designed to reflect only either 42 eV or 52 eV EUV light. The second mirror is curved, and it focuses the beam onto a specimen **S** mounted on translation stages. (b) Illustration of spectrometer design consisting of a flat silver mirror **M** and curved grating **G** for analyzing the HHG spectrum.

reflection bandwidth of 1.89 eV, and it has 30 multilayers of magnesium and silicon carbide and is capped with 15 nm of aluminum. The 52 eV mirror has a 4.11 eV bandwidth with 20 multilayers consisting of zirconium and aluminum. The normal incidence mirror setup is used for high-resolution imaging with ptychography. The two mirrors also select a narrow bandwidth (ideally only one harmonic) out of the harmonic comb. A curved mirror focuses the beam onto a specimen, which then diffracts the selected harmonic onto a CCD camera (Andor iKon-L, 2048 by 2048 pixels, each 13.5  $\mu\text{m}$  in size). The specimen is mounted on high precision translation stages (Attocube two crossed ANPx101 stages and one ANPz101 vertical stage).

In configuration (b), the spectrometer consists of a flat silver mirror and a spherical diffraction grating (1200 grooves/mm, with a radius of curvature of 2 m). The angles of grazing incidence for the flat silver mirror and the spherical grating are  $13.5^\circ$  and  $10^\circ$ , respectively. The grating at this angle has an effective tangential focal length of 17 cm. The sagittal focal length is large compared to the tangential focal length, which makes the spherical grating behave like a cylindrical mirror in this configuration. The grating separates and focuses the EUV beam onto the CCD camera for analysis of the spectrum. This configuration is used to optimize the generation of circularly polarized high harmonics.

Calibration of the HHG spectrum was accomplished by fitting the spectrum to a diffraction grating model, which was described in a previous publication.<sup>53</sup> The optics of the spectrometer can be replaced by a toroidal mirror and a flat grating. The spectrometer can be converted into a monochromator using a thin slit after the grating, allowing for more flexibility to tune the photon energy of the EUV beam for energy-sensitive imaging.

The primary function of the EUV tabletop source is imaging of polarization-sensitive phenomena. We chose ptychography as the best matched imaging method for our coherent EUV source. Ptychography is a technique that uses an illuminating beam or probe to obtain a series of diffraction patterns from overlapping sample positions, which can then be used to reconstruct a scanned specimen.<sup>54</sup> Each scan position must overlap by at least 60% to ensure sufficient data redundancy.<sup>55</sup> The collected diffraction patterns from each position are then used to reconstruct both the illuminating probe and the specimen structure.<sup>44,46</sup>

The probe in our ptychographic experiment ranges from a few micrometers to tens of micrometers in diameter, depending on the sample position with respect to the beam focus. Beam instabilities are significant with beams this small, and this is especially true with HHG sources, which are driven with such extreme nonlinear processes. Beam intensity variations and pointing instability must be addressed. Several methods are employed to reduce the instabilities.<sup>51,52</sup> We built an enclosure around the IR beam to minimize changes in air flow along the beam path, which reduces a few of these instabilities. For shorter scans, the pointing instabilities are negligible. If longer scans are required, we implement orthogonal probe relaxation techniques in our ptychographic reconstructions.<sup>47,51</sup>

The spatial step size of the sample is on the order of 1–5  $\mu\text{m}$ . We use the Python module Tike to perform the reconstruction.<sup>56</sup> Tike contains algorithms that correct for temporally varying probe, positional errors, and spatially incoherent beams. Tike was primarily designed to be implemented at synchrotron sources. To

our knowledge, this is the first time that Tike was used with a HHG EUV source.

### III. RESULTS

Here, we present the optimized spectrum of the tabletop source, particularly for the 42 and 52 eV harmonics. The multilayer mirror configuration was used to optimize for each of these harmonics, and the specimen stage was removed. The power of the beam was calculated using  $P = N_\gamma E[J]/t$ , where  $P$  is the power,  $N_\gamma$  is the total number of photons calculated by converting the counts on the camera to photons as described by Janesick *et al.* and Schlotter,<sup>57,58</sup>  $E[J]$  is the energy per photon in joules, and  $t$  is the exposure time on the CCD camera. The power of the 42 eV beam recorded on the CCD

detector was 19.4 nW. The phase-matching parameters were as follows: a laser pulse energy of 1.53 mJ at a 1 kHz repetition rate, an argon gas pressure of 12 Torr, a gas cell length of 15 mm, and a 1500 mm lens. The IR beam was filtered out using two 200 nm Al filters. The beam profile of the 42 eV beam is shown in Fig. 4(a). We could not use more IR power to optimize further because the aluminum filters would become damaged due to the high intensity of the beam. This problem can be addressed by installing silicon rejectors before the filters.<sup>59</sup>

We optimized the harmonics for 52 eV, which are near resonance with the  $M_{2,3}$  absorption edge of iron. We replaced the 1500 mm lens with a 1000 mm lens, which allows for a larger spot size, to prevent burning the aluminum filters. The power of the beam achieved for 52 eV is 8.0 nW. The phase-matching parameters for 52 eV are as follows: a laser pulse energy of 3.6 mJ at a 1 kHz repetition rate, an argon pressure of 27 Torr, and a gas cell length of 7 mm. The beam profile is shown in Fig. 4(b).

After obtaining the maximum signal for both the 42 and 52 eV harmonics, we switched our EUV configuration from multilayer mirrors to the spectrometer. We optimized the circularly polarized HHG spectrum to generate the brightest EUV spectrum with the following phase-matching parameters: a laser pulse energy of 4.16 mJ at a 1 kHz repetition rate, an argon pressure of 14 Torr, and a gas cell length of 8 mm. Using the tick markers on the rotation stages, the calcite plates were measured at  $-8^\circ$  tilt, which corresponds to a pulse delay of 600 fs, and this compensates for the quarter-wave plate and the 3 mm fused silica entrance window into the vacuum

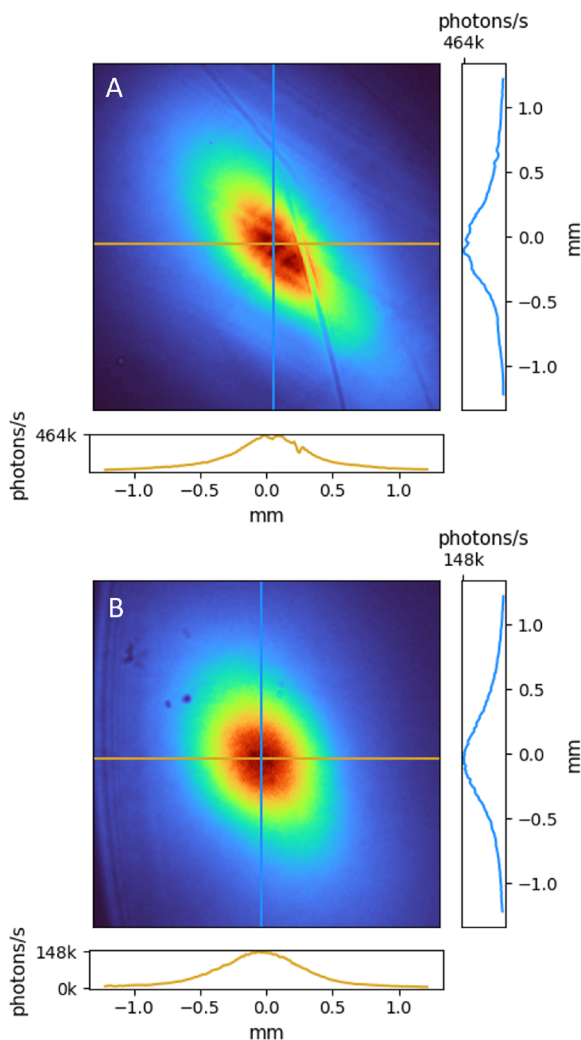


**FIG. 4.** Beam profiles of the (a) 42 eV and (b) 52 eV harmonics on the EUV CCD. Lineouts are taken from both beam profiles indicated in the gold and blue lines on each image. The lines in (a) are the defects in the aluminum filters, and the spots in (b) are the dust on the optics or detector.

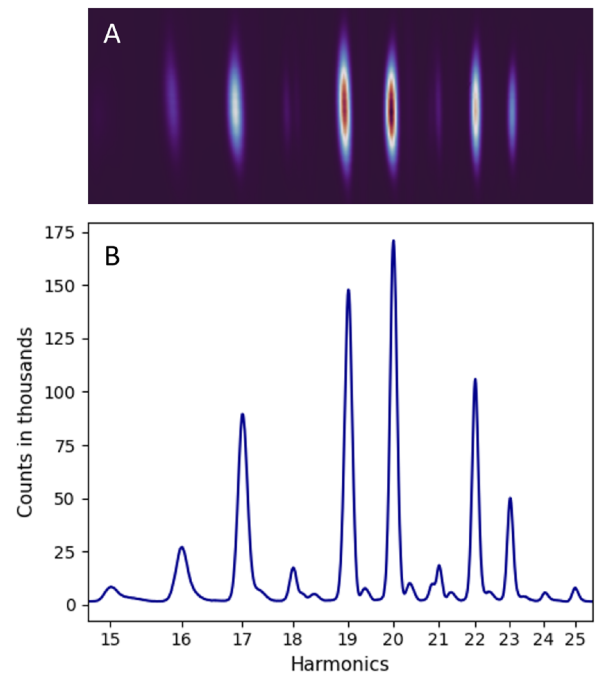


**FIG. 5.** (a) Image of the circularly polarized HHG spectrum on the EUV CCD. (b) Full vertical bin of (a). Every third harmonic is suppressed, which is a characteristic of a circularly polarized HHG beam. The harmonic orders are identified along the horizontal axis.



chamber. The optimized circularly polarized HHG spectrum is shown in Fig. 5. The spectrum in Fig. 5 shows that the circularly polarized spectrum has harmonic pairs, with every third harmonic being suppressed, which is an indicator that the harmonics are indeed circularly polarized.<sup>37,39,41</sup> The ellipticity of circularly polarized high harmonic beams was previously determined by Fleischer *et al.*<sup>37</sup>

To calibrate the spectrum, we compared circular (MAZEL-TOV inserted) and linear (MAZEL-TOV removed) spectra. The phase-matching parameters were not adjusted between the linear and circular spectra. A conventional (linearly polarized) HHG spectrum produces only odd harmonics, which can be used to identify

the odd harmonics of the circular spectrum. A 100 nm thick iron filter (Lebow Company, 10 mm aperture diameter, part No. 0.1Fe-0-C1.0mm) and a 200 nm thick zirconium filter (Lebow Company, 10 mm aperture diameter, part number 0.2Zr-0-C1.0mm) were used to calibrate the HHG spectra with the results shown in Fig. 6. The transmission curve for iron in Fig. 6 was obtained from the measured absorption indices taken at the Advanced Light Source.<sup>53</sup> The calibrated spectra are shown in Fig. 7 with the 52.7 eV  $M_{2,3}$  absorption edge of iron indicated. It is important to note that in order to obtain the brightest circularly polarized spectrum, the compression of the pulse needed to be adjusted.

We returned to the normal-incidence EUV setup for the ptychography experiment using the 42 eV beam with the MAZEL-TOV removed. Between calibrating the EUV spectrum and the ptychographic experiment, we installed silicon rejectors (KMLabs) between

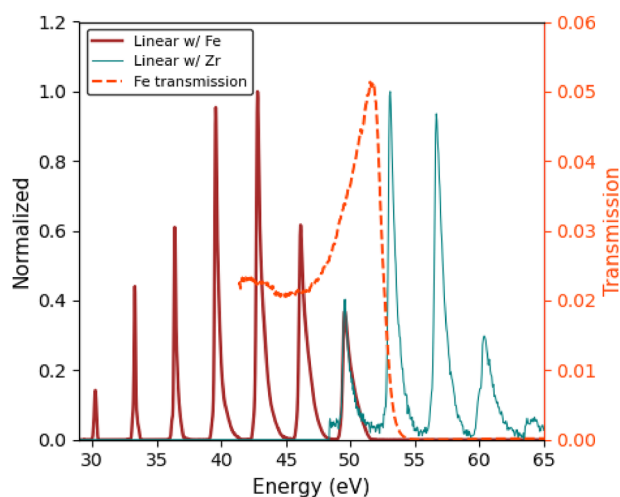


**FIG. 6.** Linearly polarized HHG spectrum. A 100 nm thick iron filter and a 200 nm thick zirconium filter were inserted separately to calibrate the harmonic spectrum. The transmission curve of iron is shown as a dotted red-orange line.

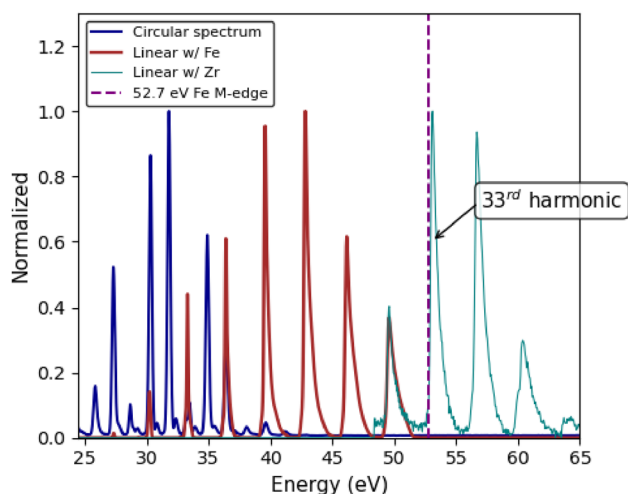


**FIG. 7.** Calibrated HHG spectra. The plot contains both linearly and circularly polarized harmonics. The 52.7 eV point, indicated as a purple dashed line, is the  $M_{2,3}$  absorption edge of iron.

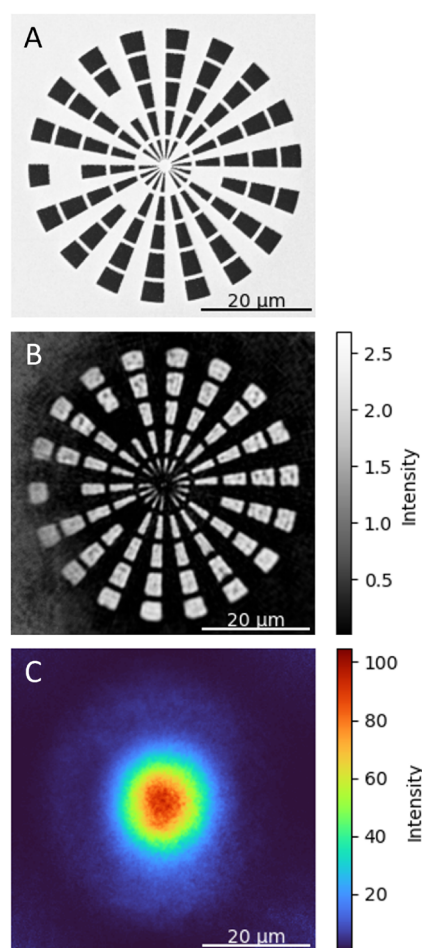


**FIG. 8.** (a) Scanning electron microscope image of the Siemens star test target. It consists of 18 spokes with 4 rings to support the structural integrity of the specimen. The largest and smallest diameters of the star are 50 and 2.3  $\mu\text{m}$ , respectively. The smallest feature of the star is 140 nm. Dark and bright regions are the free space and opaque substrate, respectively. (b) Reconstructed Siemens star using ptychography with a reconstructed pixel size of 69 nm. (c) Beam profile obtained by taking the magnitude squared of the reconstructed probe.

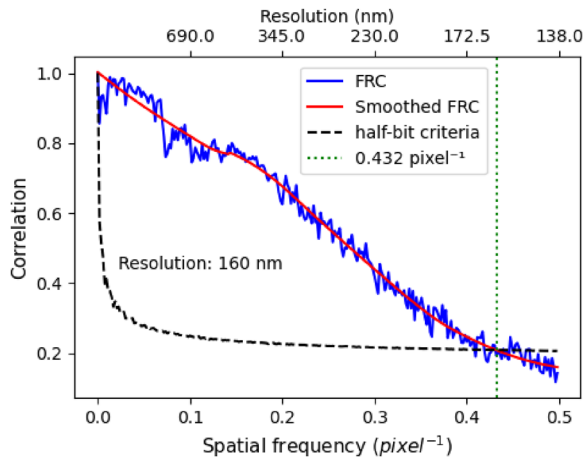


**FIG. 9.** Plot of the FRC of the reconstructed Siemens star shown as the blue curve. The FRC was smoothed using locally weighted regression<sup>64</sup> for easier determination of the resolution and is shown as the red curve. The threshold criteria for determining the resolution is half-bit, shown as a black dashed line.<sup>63</sup> Results show a resolution of 160 nm.

the gas cell and the aluminum filters. Note that the rejectors are not shown in Fig. 1. The rejectors are effective at separating the IR and EUV beams, allowing for higher driving fundamental laser power for the HHG process. We placed a 500  $\mu\text{m}$  pinhole 84 cm before the focusing mirror, measured from the curved mirror to the flat mirror and from the flat mirror to the pinhole, to both spatially filter the EUV beam and define a structured probe.<sup>60</sup> The sample-to-detector distance was 62 mm, and the specimen was placed  $\sim 10$  mm before the focus of the EUV beam. The beam size was  $\sim 20$   $\mu\text{m}$  in diameter (beam diameter at  $1/e^2$ ).

We used a Siemens star pattern as a test specimen to determine the resolution of the imaging system. The specimen was created at Brigham Young University (BYU) by coating a 100 nm thick silicon nitride window with  $\sim 40$  nm of gold. A Siemens star pattern was then milled through the gold-coated silicon nitride window using a focused Ga-ion beam. A scanning electron microscope image of the Siemens star is shown in Fig. 8(a). We scanned over the Siemens star using a 2  $\mu\text{m}$  step in a Fermat spiral pattern.<sup>61</sup> Using the regularized ptychographic iterative engine (rPIE)<sup>46</sup> algorithm and position correction in the Tike python module, we performed 6500 iterations of the algorithm to reconstruct the Siemens star and illumination probe from the collected data, with the results shown in Figs. 8(b) and 8(c), respectively.

The resolution was determined using the Fourier ring correlation (FRC) method.<sup>62,63</sup> We calculated the FRC using reconstructions from two independent datasets of the Siemens star, which gave a resolution of 160 nm, as shown in Fig. 9.

#### IV. CONCLUSION

We have developed a compact tabletop EUV source, demonstrated that it can produce circularly polarized EUV light, and calibrated the spectrum. We have optimized the system to generate both the 42 and 52 eV harmonics, producing beams with a power of 19.4 and 8.0 nW, respectively, in linear polarization mode. We have

shown that circularly polarized EUV light has been generated, which is necessary for magnetic contrast imaging of magnetic domains using MCD principles. Due to the mixture of IR and blue beams, the circularly polarized harmonics are more optimal for lower photon energies. Thus, further work needs to be done in generating higher energy harmonics for the circularly polarized spectrum. This could be done by replacing the argon gas with a medium that has a higher ionization potential, such as neon or helium.

Furthermore, we successfully demonstrated ptychographic microscopy with our HHG source using the 42 eV linearly polarized harmonic, achieving 160 nm resolution with FRC. A resolution of 160 nm should be sufficient to image thin-film magnetic samples, which can have magnetic domain walls that are several hundred nanometers across.<sup>16</sup> The system is currently designed for transmission of EUV light, which works well for thin specimens, although we plan to include an option for reflection ptychography to obtain magnetic contrast for specimens that are too thick for EUV penetration. The successful ptychographic reconstruction with linearly polarized EUV light demonstrates the capability to perform magnetic contrast imaging using MLD and linear dichroism for antiferromagnetic and ferroelectric materials, respectively. In order to obtain magnetic contrast in a ferromagnetic material using MCD, a successful reconstruction using a circularly polarized EUV beam will need to be accomplished.

#### ACKNOWLEDGMENTS

The funding was provided by the Department of Physics and Astronomy and the College of Computational, Mathematical, and Physical Sciences at Brigham Young University. We acknowledge the BYU Electron Microscopy Facility for providing access to the equipment and expertise that allowed this project to be performed. We acknowledge Dr. Justin Peatross at BYU for providing the equipment and collaboration for the tabletop EUV source.

#### AUTHOR DECLARATIONS

##### Conflict of Interest

The authors have no conflicts to disclose.

#### Author Contributions

**Taylor J. Buckway:** Conceptualization (supporting); Data curation (lead); Formal analysis (lead); Investigation (lead); Methodology (lead); Project administration (equal); Resources (equal); Software (lead); Supervision (supporting); Validation (lead); Visualization (lead); Writing – original draft (lead); Writing – review & editing (equal). **Aaron Redd:** Data curation (supporting); Formal analysis (supporting); Investigation (supporting); Methodology (supporting); Software (supporting); Writing – review & editing (equal). **Hyrum Taylor:** Data curation (supporting); Formal analysis (supporting); Investigation (supporting); Methodology (supporting); Software (supporting); Writing – review & editing (equal). **Jacob Feltman:** Resources (equal); Writing – review & editing (equal). **Kaylee Nyborg:** Investigation (supporting); Methodology (supporting); Resources (supporting); Writing – review & editing (equal). **J. Nicholas Porter:** Software (supporting); Writing – review &

editing (equal). **Joshua A. Miller:** Resources (equal); Writing – review & editing (equal). **David Allred:** Conceptualization (supporting); Funding acquisition (supporting); Methodology (supporting); Project administration (equal); Resources (equal); Supervision (equal); Writing – review & editing (equal). **Richard L. Sandberg:** Conceptualization (lead); Funding acquisition (lead); Methodology (supporting); Project administration (lead); Resources (equal); Supervision (lead); Validation (supporting); Writing – review & editing (equal).

## DATA AVAILABILITY

The data that support the findings of this study are available from the corresponding author upon reasonable request.

## APPENDIX: ALIGNMENT OF THE MAZEL-TOV

Here, we describe the alignment process for the MAZEL-TOV apparatus. The MAZEL-TOV apparatus was designed by Oren Cohen's group at Technion University.<sup>39</sup> The MAZEL-TOV consists of four optical components: a BBO crystal, two calcite compensation plates, and a dual-band quarter-wave plate designed for 800 and 400 nm wavelengths. The BBO crystal converts a portion of the IR beam into blue light. The purpose of the calcite plates is to precompensate for the pulse delay between the IR and blue pulses. The IR and blue pulses must be temporally aligned to produce the circularly polarized HHG beam. The blue pulse will experience a higher index of refraction compared to the IR beam as it passes through the quarter-wave plate and the entrance window of the vacuum chamber. The calcite plates advance the IR pulses ahead of the blue pulses to precompensate for this pulse delay. The quarter-wave plate converts the o-polarized IR beam and the e-polarized blue beam into circularly polarized beams, with each color having the opposite polarization with respect to the other. A diagram of the MAZEL-TOV is shown in Fig. 10.

Here, we present the steps for alignment of the MAZEL-TOV:

1. Insert the BBO crystal into the path of the focusing beam. The beam passes through the lens first before going into the BBO crystal to ensure that the IR and blue beams focus at the same place. As depicted in Fig. 11, we use a dichroic mirror to split

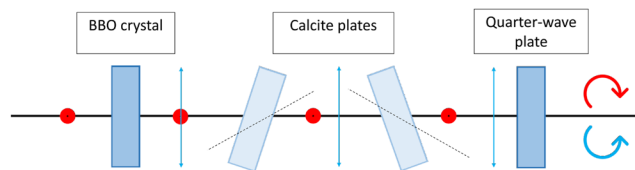


**FIG. 10.** Diagram of the MAZEL-TOV apparatus. An o-polarized IR beam is focused into the apparatus, which contains a BBO crystal, two calcite compensation plates, and a dual-band quarter-wave plate. The red and blue colors represent the IR and blue pulses, respectively. The circles represent the o-polarization, and the double arrows represent the e-polarization. The curved arrows represent the circular polarization. The IR pulses are advanced ahead of the blue pulses as they pass through the calcite plates and then are temporally realigned when they pass through the quarter-wave plate and entrance window (not shown).

the IR and blue beams. Insert a linear polarizer in each beam path, followed by a thermal power meter after each polarizer to measure the transmitted intensity. The linear polarizer in the IR beam path should be oriented such that only the o-polarized component should pass through, while the linear polarizer along the blue beam path should be oriented to allow only e-polarized light through. Adjust the orientation of the BBO crystal so that the IR beam remains purely o-polarized and the blue beam remains e-polarized, which will be required in order to adjust the delays between the IR and blue pulses with the calcite crystals. The correct polarization is confirmed when the power meter reads a maximum for both beams.

2. Insert each calcite plate individually and use the same dichroic mirror setup. The calcite crystals should be inserted in rotation mounts for precise orientation. The mounts are then attached to rotation stages for tilting the calcite crystals. The IR beam must be along the ordinary axis of the calcite crystal, while the blue beam is along the extraordinary axis. Use the branched beams, as depicted in Fig. 11, to correctly orient the calcite crystals. Begin with the first crystal and adjust its orientation until the power signals in both branches reach their maximum, indicating proper alignment. Repeat this process for the second crystal, but reverse its orientation by  $180^\circ$  relative to the first crystal, as shown by the dotted lines in Fig. 10.

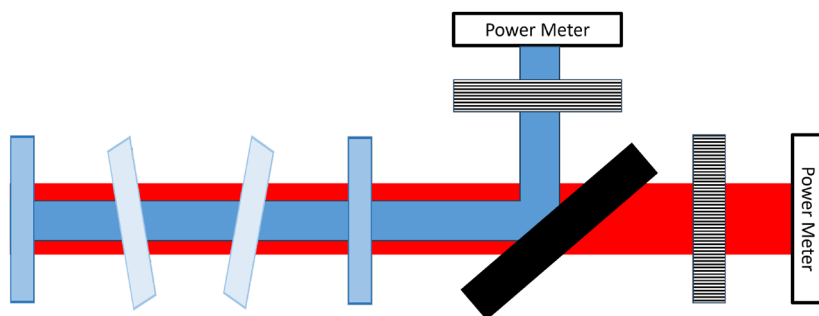


**FIG. 11.** Verifying alignment of fundamental and second harmonic beams for successful alignment of the MAZEL-TOV. The blue and light blue optics are the MAZEL-TOV components. The black rectangle is a dichroic mirror that reflects the blue and transmits the IR. The rectangle with a line along the long axis of the box is a polarizer along the e-polarized direction, while the other box with lines along the short axis is a polarizer along the o-polarized direction. Power meters are placed at the ends of each branch to measure transmitted intensity.



This inverse orientation ensures that both beams experience the same delay compensation, and this allows the blue beam to be realigned spatially with the red beam. Tilting the calcite plates adjusts the refractive index experienced by the blue beam. Due to the negative birefringence of calcite, the blue beam propagates faster than the red beam. The tilt adjustment compensates for the temporal mismatch between the IR and blue pulses as they pass through the quarter-wave plate and the fused silica entrance window of the vacuum system. To find the normal incidence angle to the calcite crystals, use the back reflection of the blue beam. Both calcite plates must be tilted at the same angle to ensure that the IR and blue beams experience identical compensation, allowing for proper temporal realignment of the blue pulses with the IR pulses.

3. Insert a dual-band quarter-wave plate after the calcite plates, oriented such that the IR and blue beams will transform from bi-linearly polarized to bi-circularly polarized beams. Use the dichroic mirror system depicted in Fig. 11 to ensure the power reading is the same for any orientation of the linear polarizer (indicating circular beam polarization).
4. Remove the beam splitter, linear polarizers, and power meters. Propagate the bi-circular beam into the gas cell to generate the circular harmonics. Use the EUV spectrometer configuration as depicted in Fig. 3(b) to observe the high harmonic spectrum. Tune the phase-matching parameters if necessary, then tilt the calcite plates until every third harmonic is suppressed (see Fig. 5), indicating proper alignment of the MAZEL-TOV.

## REFERENCES

- <sup>1</sup>D. Attwood and A. Sakdinawat, *X-Rays and Extreme Ultraviolet Radiation: Principles and Applications*, 2nd ed. (Cambridge University Press, 2017).
- <sup>2</sup>H. Levinson, "The era of high-NA EUV lithography has arrived!," *J. Micro/Nanopatterning, Mater., Metrol.* **24**, 010101 (2025).
- <sup>3</sup>APS Press Office, "Nobel Prize in Physics awarded for techniques to produce ultrashort pulses of light," *American Physical Society*, Oct. 3, 2023, <https://www.aps.org/about/news/2023/10/nobel-prize-physics>.
- <sup>4</sup>J. F. MacKay, C. Teichert, D. E. Savage, and M. G. Lagally, "Element specific magnetization of buried interfaces probed by diffuse x-ray resonant magnetic scattering," *Phys. Rev. Lett.* **77**, 3925–3928 (1996).
- <sup>5</sup>E. R. Shanblatt, C. L. Porter, D. F. Gardner, G. F. Mancini, R. M. Karl, M. D. Tanksalvala, C. S. Bevis, V. H. Vartanian, H. C. Kapteyn, D. E. Adams, and M. M. Murnane, "Quantitative chemically specific coherent diffractive imaging of reactions at buried interfaces with few nanometer precision," *Nano Lett.* **16**, 5444–5450 (2016).
- <sup>6</sup>J. Stöhr and H. C. Siegmund, *Magnetism: From Fundamentals to Nanoscale Dynamics*, 1 (Springer, 2006), p. 838.
- <sup>7</sup>P. Fischer and H. Ohldag, "X-rays and magnetism," *Rep. Prog. Phys.* **78**, 094501 (2015).
- <sup>8</sup>A. Tripathi, J. Mohanty, S. H. Dietze, O. G. Shpyrko, E. Shipton, E. E. Fullerton, S. S. Kim, and I. McNulty, "Dichroic coherent diffractive imaging," *Proc. Natl. Acad. Sci. U. S. A.* **108**, 13393–13398 (2011).
- <sup>9</sup>A. Rana, C. T. Liao, E. Iacocca, J. Zou, M. Pham, X. Lu, E. E. C. Subramanian, Y. H. Lo, S. A. Ryan, C. S. Bevis, R. M. Karl, A. J. Glaid, J. Rable, P. Mahale, J. Hirst, T. Ostler, W. Liu, C. M. O'Leary, Y. S. Yu, K. Bustillo, H. Ohldag, D. A. Shapiro, S. Yazdi, T. E. Mallouk, S. J. Osher, H. C. Kapteyn, V. H. Crespi, J. V. Badding, Y. Tserkovnyak, M. M. Murnane, and J. Miao, "Three-dimensional topological magnetic monopoles and their interactions in a ferromagnetic meta-lattice," *Nat. Nanotechnol.* **18**(3), 227–232 (2023).
- <sup>10</sup>F. Nolting, A. Scholl, J. Stöhr, J. W. Seo, J. Fompeyrine, H. Siegwart, J.-P. Locquet, S. Anders, J. Lüning, E. E. Fullerton, M. F. Toney, M. R. Scheinfein, and H. A. Padmore, "Direct observation of the alignment of ferromagnetic spins by antiferromagnetic spins," *Nature* **405**, 767–769 (2000).
- <sup>11</sup>C. Gutt, T. Sant, D. Ksenzov, F. Capotondi, E. Pedersoli, L. Raimondi, I. P. Nikolov, M. Kiskinova, S. Jaiswal, G. Jakob, M. Kläui, H. Zabel, and U. Pietsch, "Probing ultrafast changes of spin and charge density profiles with resonant XUV magnetic reflectivity at the free-electron laser fermi," *Struct. Dyn.* **4**, 055101 (2017).
- <sup>12</sup>S. Polisetty, J. Zhou, J. Karthik, A. R. Damodaran, D. Chen, A. Scholl, L. W. Martin, and M. Holcomb, "X-ray linear dichroism dependence on ferroelectric polarization," *J. Phys.: Condens. Matter* **24**, 245902 (2012).
- <sup>13</sup>Y. Esashi, N. W. Jenkins, Y. Shao, J. M. Shaw, S. Park, M. M. Murnane, H. C. Kapteyn, and M. Tanksalvala, "Tabletop extreme ultraviolet reflectometer for quantitative nanoscale reflectometry, scatterometry, and imaging," *Rev. Sci. Instrum.* **94**, 123705 (2023).
- <sup>14</sup>T. Fan, P. Grychtol, R. Knut, C. Hernández-García, D. D. Hickstein, D. Zusin, C. Gentry, F. J. Dolla, C. A. Mancuso, C. W. Hogle, O. Kfir, D. Legut, K. Carva, J. L. Ellis, K. M. Dorney, C. Chen, O. G. Shpyrko, E. E. Fullerton, O. Cohen, P. M. Oppeneer, D. B. Milošević, A. Becker, A. A. Jaroń-Becker, T. Popmintchev, M. M. Murnane, and H. C. Kapteyn, "Bright circularly polarized soft x-ray high harmonics for x-ray magnetic circular dichroism," *Proc. Natl. Acad. Sci. U. S. A.* **112**, 14206–14211 (2015).
- <sup>15</sup>P. C. Johnsen, S. A. Ryan, C. Gentry, A. Grafov, H. Kapteyn, and M. Murnane, "A beamline for ultrafast extreme ultraviolet magneto-optical spectroscopy in reflection near the shot noise limit," *Rev. Sci. Instrum.* **94**, 033001 (2023).
- <sup>16</sup>O. Kfir, S. Zayko, C. Nolte, M. Sivas, M. Möller, B. Hebler, S. S. P. K. Arekapudi, D. Steil, S. Schäfer, M. Albrecht, O. Cohen, S. Mathias, and C. Ropers, "Nanoscale magnetic imaging using circularly polarized high-harmonic radiation," *Sci. Adv.* **3**, ea04641 (2017).
- <sup>17</sup>C. La-O-Vorakiat, M. Siemens, M. M. Murnane, H. C. Kapteyn, S. Mathias, M. Aeschlimann, P. Grychtol, R. Adam, C. M. Schneider, J. M. Shaw, H. Nembach, and T. J. Silva, "Ultrafast demagnetization dynamics at the M edges of magnetic elements observed using a tabletop high-harmonic soft x-ray source," *Phys. Rev. Lett.* **103**, 257402 (2009).
- <sup>18</sup>S. Mathias, C. La-O-Vorakiat, P. Grychtol, P. Granitzka, E. Turgut, J. M. Shaw, R. Adam, H. T. Nembach, M. E. Siemens, S. Eich, C. M. Schneider, T. J. Silva, M. Aeschlimann, M. M. Murnane, and H. C. Kapteyn, "Probing the timescale of the exchange interaction in a ferromagnetic alloy," *Proc. Natl. Acad. Sci. U. S. A.* **109**, 4792–4797 (2012).
- <sup>19</sup>M. D. Seaberg, D. E. Adams, E. L. Townsend, D. A. Raymondson, W. F. Schlotter, Y. Liu, C. S. Menoni, L. Rong, C.-C. Chen, J. Miao, H. C. Kapteyn, and M. M. Murnane, "Ultrahigh 22 nm resolution coherent diffractive imaging using a desktop 13 nm high harmonic source," *Opt. Express* **19**, 22470–22479 (2011).
- <sup>20</sup>R. L. Sandberg, C. Song, P. W. Wachulak, D. A. Raymondson, A. Paul, B. Amirbekian, E. Lee, A. E. Sakdinawat, C. La-O-Vorakiat, M. C. Marconi, C. S. Menoni, M. M. Murnane, J. J. Rocca, H. C. Kapteyn, and J. Miao, "High numerical aperture tabletop soft x-ray diffraction microscopy with 70-nm resolution," *Proc. Natl. Acad. Sci. U. S. A.* **105**(1), 24–27 (2008).
- <sup>21</sup>P. B. Corkum, "Plasma perspective on strong field multiphoton ionization," *Phys. Rev. Lett.* **71**, 1994–1997 (1993).
- <sup>22</sup>E. Takahashi, Y. Nabekawa, and K. Midorikawa, "Generation of 10- $\mu$ J coherent extreme-ultraviolet light by use of high-order harmonics," *Opt. Lett.* **27**, 1920 (2002).
- <sup>23</sup>H. C. Kapteyn, M. M. Murnane, and I. P. Christov, "Extreme non-linear optics: Coherent x rays from lasers," *Phys. Today* **58**(3), 39–46 (2005).
- <sup>24</sup>E. Constant, D. Garzella, P. Breger, E. Mével, C. Dorrer, C. Le Blanc, F. Salin, and P. Agostini, "Optimizing high harmonic generation in absorbing gases: Model and experiment," *Phys. Rev. Lett.* **82**, 1668–1671 (1999).
- <sup>25</sup>T. Popmintchev, "Tunable ultrafast coherent light in the soft and hard x-ray regions of the spectrum: Phase matching of extreme high-order harmonic generation," Ph.D. thesis, University of Colorado at Boulder, 2010.

- <sup>26</sup>A. L. Lytle, "Phase matching and coherence of high-order harmonic generation in hollow waveguides," Ph.D. thesis, University of Colorado, 2001.
- <sup>27</sup>E. Takahashi, Y. Nabekawa, T. Otsuka, M. Obara, and K. Midorikawa, "Generation of highly coherent submicrojoule soft x rays by high-order harmonics," *Phys. Rev. A* **66**, 021802 (2002).
- <sup>28</sup>F. Brizuela, C. M. Heyl, P. Rudawski, D. Kroon, L. Rading, J. M. Dahlström, J. Mauritsson, P. Johnsson, C. L. Arnold, and A. L'Huillier, "Efficient high-order harmonic generation boosted by below-threshold harmonics," *Sci. Rep.* **3**, 1410 (2013).
- <sup>29</sup>R. Budriunas, "Collinear setup for two-color high harmonic generation," Bachelor's thesis, Lund University, 2013.
- <sup>30</sup>C. H. Nam, I. J. Kim, C. M. Kim, H. T. Kim, and G. H. Lee, *Generation of Exceptionally Strong Harmonics from He in an Orthogonally Polarized two-color Laser Field* (Springer, New York, 2007), pp. 435–441.
- <sup>31</sup>J. Rothhardt, M. Krebs, S. Hädrich, S. Demmler, J. Limpert, and A. Tünnermann, "Absorption-limited and phase-matched high harmonic generation in the tight focusing regime," *New J. Phys.* **16**, 033022 (2014).
- <sup>32</sup>P. Rudawski, C. M. Heyl, F. Brizuela, J. Schwenke, A. Persson, E. Mansten, R. Rakowski, L. Rading, F. Campi, B. Kim, P. Johnsson, and A. L'Huillier, "A high-flux high-order harmonic source," *Rev. Sci. Instrum.* **84**, 073103 (2013).
- <sup>33</sup>E. J. Takahashi, Y. Nabekawa, H. Mashiko, H. Hasegawa, A. Suda, and K. Midorikawa, "Generation of strong optical field in soft x-ray region by using high-order harmonics," *IEEE J. Sel. Top. Quantum Electron.* **10**, 1315–1328 (2004).
- <sup>34</sup>J. Zhou, J. Peatross, M. M. Murnane, H. C. Kapteyn, and I. P. Christov, "Enhanced high-harmonic generation using 25 fs laser pulses," *Phys. Rev. Lett.* **76**, 752–755 (1996).
- <sup>35</sup>M. Odstrčil, P. Baksh, H. Kim, S. A. Boden, W. S. Brocklesby, and J. G. Frey, "Ultra-broadband ptychography with self-consistent coherence estimation from a high harmonic source," *Proc. SPIE* **9589**, 958912 (2015).
- <sup>36</sup>P. D. Baksh, M. Odstrčil, H.-S. Kim, S. A. Boden, J. G. Frey, and W. S. Brocklesby, "Wide-field broadband extreme ultraviolet transmission ptychography using a high-harmonic source," *Opt. Lett.* **41**(7), 1317–1320 (2016).
- <sup>37</sup>A. Fleischer, O. Kfir, T. Diskin, P. Sidorenko, and O. Cohen, "Spin angular momentum and tunable polarization in high-harmonic generation," *Nat. Photonics* **8**, 543–549 (2014).
- <sup>38</sup>O. Kfir, P. Grychtol, E. Turgut, R. Knut, D. Zusin, D. Popmintchev, T. Popmintchev, H. Nembach, J. M. Shaw, A. Fleischer, H. Kapteyn, M. Murnane, and O. Cohen, "Generation of bright phase-matched circularly-polarized extreme ultraviolet high harmonics," *Nat. Photonics* **9**, 99–105 (2015).
- <sup>39</sup>O. Kfir, E. Bordo, G. Ilan Haham, O. Lahav, A. Fleischer, and O. Cohen, "In-line production of a bi-circular field for generation of helically polarized high-order harmonics," *Appl. Phys. Lett.* **108**, 211106 (2016).
- <sup>40</sup>S. Zayko, O. Kfir, M. Heigl, M. Lohmann, M. Sivils, M. Albrecht, and C. Ropers, "Ultrafast high-harmonic nanoscopy of magnetization dynamics," *Nat. Commun.* **12**, 6337 (2021).
- <sup>41</sup>S. Long, W. Becker, and J. K. McIver, "Model calculations of polarization-dependent two-color high-harmonic generation," *Phys. Rev. A* **52**, 2262–2278 (1995).
- <sup>42</sup>C. La-O-Vorakiat, E. Turgut, C. A. Teale, H. C. Kapteyn, M. M. Murnane, S. Mathias, M. Aeschlimann, C. M. Schneider, J. M. Shaw, H. T. Nembach, and T. J. Silva, "Ultrafast demagnetization measurements using extreme ultraviolet light: Comparison of electronic and magnetic contributions," *Phys. Rev. X* **2**, 011005 (2012).
- <sup>43</sup>J. M. Rodenburg and H. M. L. Faulkner, "A phase retrieval algorithm for shifting illumination," *Appl. Phys. Lett.* **85**, 4795–4797 (2004).
- <sup>44</sup>P. Thibault, M. Dierolf, O. Bunk, A. Menzel, and F. Pfeiffer, "Probe retrieval in ptychographic coherent diffractive imaging," *Ultramicroscopy* **109**, 338–343 (2009).
- <sup>45</sup>P. Thibault and M. Guizar-Sicairos, "Maximum-likelihood refinement for coherent diffractive imaging," *New J. Phys.* **14**, 063004 (2012).
- <sup>46</sup>A. Maiden, D. Johnson, and P. Li, "Further improvements to the ptychographical iterative engine," *Optica* **4**, 736–745 (2017).
- <sup>47</sup>M. Odstrčil, A. Menzel, and M. Guizar-Sicairos, "Iterative least-squares solver for generalized maximum-likelihood ptychography," *Opt. Express* **26**, 3108 (2018).
- <sup>48</sup>C. Donnelly, V. Scagnoli, M. Guizar-Sicairos, M. Holler, F. Wilhelm, F. Guillou, A. Rogalev, C. Detlefs, A. Menzel, J. Raabe, and L. J. Heyderman, "High-resolution hard x-ray magnetic imaging with dichroic ptychography," *Phys. Rev. B* **94**, 064421 (2016).
- <sup>49</sup>M. Di Pietro Martínez, A. Wartelle, N. Mille, S. Stanesco, R. Belkhou, F. Fettaf, V. Favre-Nicolin, and G. Beutier, "Magnetic x-ray imaging using a single polarization and multimodal ptychography," *Phys. Rev. Lett.* **134**, 016704 (2025).
- <sup>50</sup>H. M. L. Faulkner and J. M. Rodenburg, "Error tolerance of an iterative phase retrieval algorithm for moveable illumination microscopy," *Ultramicroscopy* **103**, 153–164 (2005).
- <sup>51</sup>M. Odstrčil, P. Baksh, S. A. Boden, R. Card, J. E. Chad, J. G. Frey, W. S. Brocklesby, J. Miao, P. Charalambous, J. Kirz, and D. Sayre, "Ptychographic coherent diffractive imaging with orthogonal probe relaxation," *Opt. Express* **24**(8), 8360–8369 (2016).
- <sup>52</sup>P. Thibault and A. Menzel, "Reconstructing state mixtures from diffraction measurements," *Nature* **494**, 68–71 (2013).
- <sup>53</sup>T. J. Buckway, A. Redd, D. Lewis, E. Gullikson, J. Vawdrey, K. Chesnel, D. Allred, and R. L. Sandberg, "Addressing calibration of high-harmonic generation sources used for studying magnetism," *Proc. SPIE* **12694**, 1269404 (2023).
- <sup>54</sup>M. Guizar-Sicairos and J. R. Fienup, "Phase retrieval with transverse translation diversity: A nonlinear optimization approach," *Opt. Express* **16**(10), 7264–7278 (2008).
- <sup>55</sup>O. Bunk, M. Dierolf, S. Kynde, I. Johnson, O. Marti, and F. Pfeiffer, "Influence of the overlap parameter on the convergence of the ptychographical iterative engine," *Ultramicroscopy* **108**, 481–487 (2008).
- <sup>56</sup>D. Gursoy and D. J. Ching, "Tike," Computer Software, <https://doi.org/10.11578/dc.20230202.1>, 2022.
- <sup>57</sup>J. R. Janesick, T. Elliott, S. Collins, M. M. Blouke, and J. Freeman, "Scientific charge-coupled devices," *Opt. Eng.* **26**, 692–714 (1987).
- <sup>58</sup>W. F. Schlotter, "Lensless fourier transform holography with soft x-rays," Ph.D. thesis, Stanford University, 2007.
- <sup>59</sup>Y. Nagata, Y. Nabekawa, and K. Midorikawa, "Development of high-throughput, high-damage-threshold beam separator for 13 nm high-order harmonics," *Opt. Lett.* **31**(9), 1316–1318 (2006).
- <sup>60</sup>N. X. Truong, R. Safaei, V. Cardin, S. M. Lewis, X. L. Zhong, F. Légaré, and M. A. Denecke, "Coherent tabletop EUV ptychography of nanopatterns," *Sci. Rep.* **8**, 16693 (2018).
- <sup>61</sup>X. Huang, H. Yan, R. Harder, Y. Hwu, I. K. Robinson, Y. S. Chu, J. Rodenburg, A. Hurst, A. Cullis, B. Dobson, F. Pfeiffer, O. Bunk, C. David, K. Jefimovs, and I. Johnson, "Optimization of overlap uniformness for ptychography," *Opt. Express* **22**(10), 12634–12644 (2014).
- <sup>62</sup>M. Van Heel, "Similarity measures between images," *Ultramicroscopy* **21**, 95–100 (1987).
- <sup>63</sup>M. Van Heel and M. Schatz, "Fourier shell correlation threshold criteria," *J. Struct. Biol.* **151**, 250–262 (2005).
- <sup>64</sup>W. S. Cleveland, "Robust locally weighted regression and smoothing scatterplots," *J. Am. Stat. Assoc.* **74**, 829–836 (1979).